UoC-3: A MOF with an Anionic Framework Based on Uranyl UO_2^{2+} Nodes and Partly Fluorinated BTB Linkers

Ronja Christoffels[†], Carina Breitenbach (née Stastny)[†], Jean Patrick Weber[†], Lisa Körtgen[†], Christian Tobeck[†], Michael Wilhelm[†], Sanjay Mathur[†], Jörg-M. Neudörfl[‡], Majied Sadegh Zadeh Farid[§], Melisa Maslo[§], Erik Strub[§], and Uwe Ruschewitz[,†]*

[†] Department of Chemistry (Inorganic Chemistry), University of Cologne, Greinstraße 6, D-50939 Cologne, Germany

[‡] Department of Chemistry (Organic Chemistry), University of Cologne, Greinstraße 4, D-50939 Cologne, Germany

[§] Division of Nuclear Chemistry, University of Cologne, Zülpicher Straße 45, D-50674 Cologne, Germany and Nuclear Chemistry (INM-5), Forschungszentrum Jülich, D-52425 Jülich, Germany

KEYWORDS. Anionic Framework • Cation Exchange • Fluorinated Ligand • MOF • Uranium

ABSTRACT. Reaction of $UO_2(NO_3)_2 \cdot 6\ H_2O$ with partly fluorinated H_3-*3F*-BTB (BTB^{3-}: benzene-1,3,5-tribenzoate) in DMF leads to the crystallization of the MOF $[(CH_3)_2NH_2][UO_2($*3F*-

BTB)] · x DMF, named UoC-3 (UoC: University of Cologne). X-ray single crystal structure analysis (*Pnna*, $Z = 4$) reveals that an anionic framework is formed, in which UO_2^{2+} nodes are connected by *3F*-BTB^{3-} ligands. Due to the fluorination of the inner ring of the linker, its three benzoate groups are tilted to an "out of plane" arrangement, which leads to the formation of a 3D structure with large pores. This is in contrast to a known uranyl coordination polymer with the unfluorinated BTB^{3-} linker, where an almost coplanar arrangement of the linker leads to graphene-like layers. The high porosity of UoC-3 was confirmed by N_2 gas sorption measurements, resulting in S_{BET} = 4844 m^2/g. The charge compensating $[(CH_3)_2NH_2]^+$ cation is formed by hydrolysis of DMF. Direct addition of $[(CH_3)_2NH_2]Cl$ to the reaction carried out in ethanol/H_2O (v:v, 5:1) leads to the same MOF, but with lower crystallinity. When using solvents, which hydrolyze to larger cations (e.g. DEF: $[(C_2H_5)_2NH_2]^+$ and DBF: $[(C_4H_9)_2NH_2]^+$), again the formation of UoC-3 was found, as confirmed by X-ray single crystal analysis and X-ray powder diffraction. Thus, no templating-effect was achieved with these cations. The exchange of the organic cations by K^+ turned out to be successful, as revealed by XPS analysis. UoC-3 was also successfully tested to remove approx. 96% radioactive $^{137}Cs^+$ from aqueous solutions (93% after one regeneration cycle), while retaining its crystal structure.

INTRODUCTION

Since the discovery of MOF-5[1] and HKUST-1[2] in 1999, the field of metal-organic frameworks (MOFs) has experienced an enormous development. In 2017, it was reported that the Cambridge Crystallographic Data Centre (CCDC)[3] contained almost 70,000 entries that were classified as MOFs.[4] An updated MOF subset, available via the CONQUEST software of the CCDC,[5] contains

almost 106,000 entries (version 5.42, Nov. 2020). Within this updated MOF subset, 1490 entries were found that consist of uranium cations as metal nodes, among which the majority (~1200 entries) shows a U···OOC-R coordination. *Shustova* and co-workers presented an approach to classify this large number of uranium (actinide) MOFs.[6] They analyzed more than 100 crystal structures of (U,Th)-based MOFs and subdivided them into compounds with mononuclear motifs (the majority) and those with multinuclear motifs, mainly bi-, tri-, tetra-, and hexanuclear motifs. It was an intriguing aspect of this work that some of the resulting MOF structures show striking similarities with those of U-containing minerals like walpurgite, adolfpateraite, studtite or deliensite.[6] Very recent reviews on actinide MOFs show the increasing interest in this class of compounds.[7,8]

BTB^{3-} (benzene-1,3,5-tribenzoate) is a commonly used ligand for the construction of coordination polymers (CPs) and MOFs (~500 entries in the MOF subset mentioned above). MOF-177 is probably the most prominent representative, in which BTB^{3-} linkers connect Zn_4O-oxo clusters.[9] As MOFs with the BTB^{3-}linker typically result in highly porous materials, it is somewhat surprising that only two examples of U-BTB-MOFs were reported in the literature up to now. In 2015, *Wang* et al. reported a layered coordination polymer $[(CH_3)_2NH_2][UO_2(BTB)]\cdot DMF\cdot 6.5H_2O$ crystallizing in the acentric space group $P3_121$.[10] The BTB^{3-} linker is almost planar in this compound due to the aromatic sp^2 hybridization of all its carbon atoms. The UO_2^{2+} nodes are coordinated in a hexagonal bipyramidal geometry with the uranyl-oxygen atoms forming the apices and six oxygen atoms of three carboxylate groups the base of the bipyramid. This very regular coordination environment and the planarity of the linker lead to an open honeycomb-like layered structure, well-known in the literature.[11] In 2017, *Li* et al. constructed a giant MOF based on UO_2^{2+} units and a modified BTB^{3-} linker (NU-1301), where all

hydrogen atoms of the inner ring were replaced by methyl groups.[12] Due to steric repulsion, this methylation leads to a cancellation of the planarity of the Me_3-BTB^{3-} linker and increased torsion angles between the inner ring and the benzoate rings are observed, resulting in the formation of a 3D MOF with unprecedented complexity (e.g. V = 5,201,096 Å^3 and 816 uranium nodes and linkers in the unit cell).

In our ongoing research, we are interested in CPs and MOFs with fluorinated aromatic carboxylate linkers.[13,14,15,16,17,18] It was already pointed out that the fluoro substituents also have a significant influence on the torsion angles of neighboring groups.[19,20,21,22,23] In this respect, it was of interest to see how a fluorination of the inner ring of the BTB^{3-} ligand affects its planarity and – in a next step – the structural chemistry of the resulting CPs and MOFs. However, the synthesis of this ligand, named *3F*-BTB^{3-}, has not been described in the literature so far. In the following, we will describe its synthesis as well as the new MOF $[R_2NH_2][UO_2(3F\text{-BTB})] \cdot x\ L$, named UoC-3 (UoC: University of Cologne; L = DMF and R =CH_3 or L = DEF and R = C_2H_5), constructed with this linker. It is noteworthy that $[(CH_3)_2NH_2][UO_2(BTB)]\cdot DMF\cdot 6.5H_2O$,[10] NU-1301,[12] and UoC-3 form anionic frameworks.

EXPERIMENTAL SECTION

Radiation Precautions. Uranium is a natural occurring radioactive material (NORM). The amount of uranium used in this work can be handled outside a radiation protection area in compliance with German radiation protection regulations, i.e. when it is documented that the workers' annual exposition to radiation is below the limit of 1 mSv. ^{137}Cs is emitting 622 keV γ radiation and must therefore be handled in a laboratory within a radiation protection area, applying radiation

protection measures like appropriate shielding, contamination control and personal dosimetry. Especially, the ^{137}Cs stock solution should be stored in a lead shielded vial.

Linker Synthesis. The synthesis of the *3F*-BTB^{3-} linker, which is described for the first time, is given in the Supporting Information.

Synthesis of UoC-3. In a typical synthesis 0.0753 g (0.15 mmol, 1.5 eq.) $UO_2(NO_3)_2 \cdot 6\ H_2O$ and 0.0492 g (0.1 mmol, 1.0 eq.) H_3-*3F*-BTB were dissolved in a mixture of 4 ml DMF and 1 ml deionized water, after which 100 µl HNO_3 (conc.) were added. The solution was heated for 48 h at 100 °C in a Teflon® lined 20 ml pressure vessel (Parr Instrument Company) and cooled down to room temperature during 12 h. The precipitates were filtered off, washed with DMF/H_2O and dried in air to give the as-synthesized product **1**. The purity of the obtained material was confirmed by its PXRD pattern (Figure 5 and Figure S6, Supporting Information). Using other solvent mixtures, acids or additives, always MOFs with the same UoC-3 topology were obtained. In Table 1, some of these experiments are summarized. It is remarkable that even with KCl in an EtOH/H_2O mixture, a MOF with the UoC-3 topology is obtained.

Table 1. Varying reaction conditions for the synthesis of UoC-3 (DMF: *N*,*N*-dimethylformamide; DMA: *N*,*N*-dimethylacetamide; DEF: *N*,*N*-diethylformamide; DBF: *N*,*N*-di(*n*-butyl)formamide).

Solvent mixture	**Product**	**PXRD pattern**
4 ml DMF, 1 ml H_2O, 100 µl HNO_3 (conc)	$[(CH_3)_2NH_2][(UO_2)$*3F*-BTB$]$ · x solvent, **1**	Figure 5 and Figure S6 (Supporting Information)
4 ml DMA, 1 ml H_2O, 100 µl HNO_3 (conc)	$[(CH_3)_2NH_2][(UO_2)$*3F*-BTB$]$ · x solvent, **1**	
0.0815 g $[(CH_3)_2NH_2]Cl$, 5 ml EtOH, 1 ml H_2O	$[(CH_3)_2NH_2][(UO_2)$*3F*-BTB$]$ · x solvent, **1**	Figure 5

4 ml DEF, 1 ml H_2O, 100 µl HCl (conc)	$[(C_2H_5)_2NH_2][(UO_2)3F$-BTB] · x solvent, **2**	Figure S7 (Supporting Information)
4 ml 1-formylpyrrolidine, 1 ml H_2O, 100 µl HCl (conc)	$[(C_4H_8)NH_2][(UO_2)3F$-BTB] · x solvent	Figure S9 (Supporting Information)
4 ml DBF, 1 ml H_2O, 100 µl HCl (conc)	$[(C_4H_9)_2NH_2][(UO_2)3F$-BTB] · x solvent	Figure S10 (Supporting Information)
0.0373 g KCl, 1 ml H_2O, 5 ml EtOH	$K[(UO_2)3F$-BTB] · x solvent	Figure S11 (Supporting Information)

Cation exchange with K^+. 0.7455 g KCl were dissolved in 20 ml deionized water. 0.05 g $[(CH_3)_2NH_2][(UO_2)3F$-BTB] · 4 DMF (**1**) were added, and the solution was stirred for 48 h. Afterwards, the product was filtered off and washed with several portions of deionized water. PXRD measurements (Figure S12, Supporting Information) confirm that the UoC-3 framework is still intact after this procedure. Note: some of the intensities of early reflections are different to the starting material **1**, as – most likely – DMF within the pores of **1** was replaced by water leading to the observed modulation of intensities. The successful exchange of $[(CH_3)_2NH_2]^+$ by K^+ cations was proven by XPS measurements (Figure 9).

Cation exchange with radiocesium ($^{137}Cs^+$). 0.010 g of $[(CH_3)_2NH_2][(UO_2)3F$-BTB] · 4 DMF (**1**) were placed in a centrifuge tube. About 40 µL of 1M LiOH solution was added for pH adjustment. After 15 min, 100 µL of a carrier-free ^{137}Cs stock solution with an activity of about 1000 Bq/mL and 1860 µL of deionized water were added (note: addition of LiOH was necessary to prevent a degradation of the MOF as the ^{137}Cs stock solution was slightly acidic). The solution was shaken for 1 h at room temperature. After centrifugation, half of the clear supernatant was pipetted into an identical tube. The distribution coefficient K_d was determined quantifying ^{137}Cs in both tubes

with γ spectrometry using the same geometry. For the determination of the adsorption isotherm, different amounts of (non-radioactive) Cs^+ were added. For the determination of the ion selectivity, a surplus of Na^+/K^+ was added (see Table S1, Supporting Information).

X-ray Single-Crystal Structure Analysis. Single crystal data of **1** (290(2) K) and **2** (103(2) K and 280(2) K) were collected with a Bruker APEX-II CCD diffractometer (Cu Kα radiation, λ = 1.54178 Å). It was found that measurements at low temperatures decrease the quality of the single crystals significantly and little cracks are visible under the microscope. Therefore, only the data obtained at 290(2) and 280(2) K are discussed in this manuscript. Semiempirical absorption corrections were executed using SADABS-2016/2.[24] The crystal structures were solved by direct methods (SIR-92)[25] and the structural models were completed using difference Fourier maps calculated with SHELXL-2014, which was also used for all refinements.[26] All programs were run under the WinGX system.[27] All non-hydrogen atoms were refined anisotropically. Hydrogen atoms were placed on calculated positions and refined with fixed distances (C–H: 0.93 Å). Possible positions for the $R_2NH_2^+$ cations (R = CH_3, C_2H_5) were identified (Figure S4, Supporting Information), but a stable refinement of these positions could not be achieved. Therefore, these cations positions as well as the disordered solvent molecules within the pores were omitted in the final refinements, in which the SQUEEZE[28] function within PLATON[29] was used to account for their electron density. Details of the single-crystal structure analyses are given in Table 2. For the illustration of the crystal structures Diamond 4.2.0 was used.[30]

Powder X-ray Diffraction (PXRD). PXRD data were collected at room temperature on a Stoe Stadi P powder diffractometer (germanium monochromator, Mo Kα_1 radiation, λ = 0.70926 Å, Mythen detector). Samples were filled into glass capillaries (∅ = 0.3 mm). Typical recording times

were 30 min. Employing the WinXPow software suite,[31] the recorded patterns were compared with theoretical patterns calculated from known single-crystal structure data.

Elemental Analysis. Elemental analyses were performed in-house with a CHNS Euro EA 3000 Analyzer (HEKAtech GmbH).

Thermoanalytical Investigations. Differential scanning calorimetry (DSC) and thermogravimetric analyses (TGA) were performed with a Mettler Toledo Star^e TGA/DSC 1 system in a constant argon stream (30 ml/min). Samples were heated with a heating rate of 10 °C/min.

N_2 Sorption. The measurements were carried out at 77 K with an AUTOSORB-1-MP (Quantachrome). Prior to the N_2 gas sorption measurements, the samples were heated at varying temperatures (**1**: 120-220 °C; **2**: 180-220 °C) in high vacuum ($1 \cdot 10^{-7}$ mbar) for 24 h (Figures S20 and S21, Supporting Information). The Brunauer–Emmett–Teller (BET) surface area was calculated based on the pressure region $p/p_0 = 0.0005–0.03$. For both compounds, the highest surface area was obtained after activation at 200 °C for 24 h.

NMR Spectroscopy. NMR measurements were performed with a Bruker Avance II 300 spectrometer. Spectra were recorded at the following frequencies: ^{1}H NMR: 300 MHz, ^{19}F NMR: 282 MHz, ^{13}C NMR: 75 MHz. The chemical shifts (δ) are given in ppm, referenced to the respective solvent.

IR Spectroscopy. Samples were measured as pure solids on a Perkin–Elmer SPECTRUM 400 FT-IR with ATR cell under ambient conditions. For each sample, 16 scans were measured and added for the final spectrum.

Raman Spectroscopy. Raman spectra were recorded on a Renishaw InVia Quontor Raman microscope using a 457 nm laser (laser power 10%, exposure time: 10 s), which was focused on the sample with a x10 objective (grating: 3000 lines per mm). The spectrometer is equipped with a Centrus 05TJ CCD detector. Before and during the measurements the instrument was calibrated with an internal Si standard. IR and Raman spectra were visualized with Origin 8.5.0.[32]

XPS. XPS analysis was performed with an ESCA M-Probe system from Surface Science Instruments. The samples were irradiated with Al Kα rays (λ = 8.33 Å). Survey scans were recorded with a detector pass energy of 158.28 eV and high-resolution spectra were recorded with a pass energy of 55.2 eV. The binding energies of all spectra were referenced to 284.8 eV based on the C 1s spectra. All spectra were fitted using a Shirley background. C=C/C-C bindings were fitted together with an asymmetric line-shape A(0.38,0.4,20)GL(20), whereas all other peaks were fitted with a GL(30) line shape using CasaXPS software from Casa Software Ltd.

RESULTS AND DISCUSSION

The linker H_3-*3F*-BTB (1,3,5-trifluoro-2,4,6-tris(4-carboxyphenyl)benzene) was synthesized via an oxidation of the known aldehyde[33] with $KMnO_4$ (Scheme 1). The aldehyde is accessible via a palladium-catalyzed cross-coupling reaction of 1,3,5-trifluoro-2,4,6-triiodobenzene and 4-formylphenylboronic acid (for details see Supporting Information).[33] The overall yield is 79.5 % and H_3-*3F*-BTB is obtained in a phase-pure form.

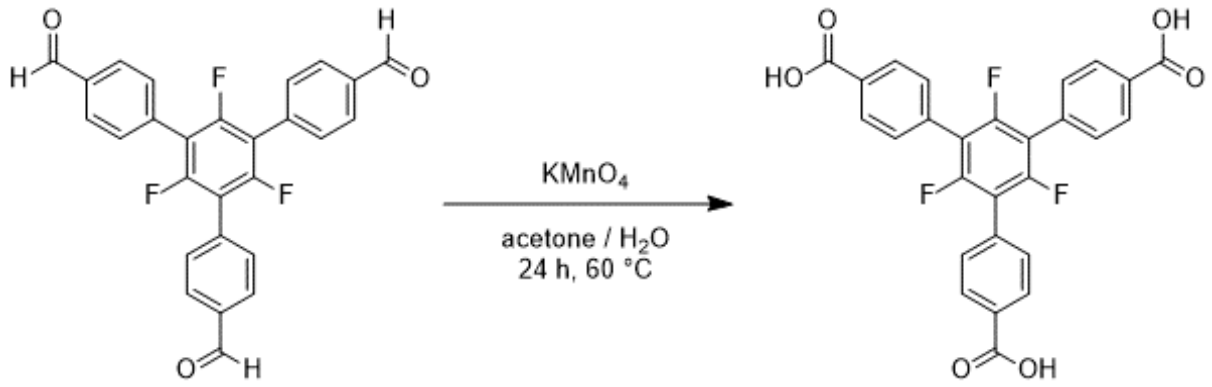

Scheme 1. Synthesis of H_3-*3F*-BTB via oxidation of the known aldehyde.[33]

By reaction of $UO_2(NO_3)_2 \cdot 6\ H_2O$ with H_3-*3F*-BTB under solvothermal conditions in DMF (for details see experimental section), yellow crystals of **1** (Figure S1, Supporting Information) were obtained, from which a single crystal suitable for an X-ray structure analysis was isolated. **1** crystallizes in the orthorhombic space group *Pnna* with $Z = 4$. The unit cell contains four UO_2^{2+} units connected by four *3F*-BTB^{3-} anions resulting in the anionic framework $[UO_2(3F\text{-}BTB)^-]_n$. The ORTEP plot of the (extended) asymmetric unit with labeling of the atoms is given in Figure 1. A difference Fourier map resulted in two positions within the pores of **1** with distances as expected for an organic cation $[(CH_3)_2NH_2]^+$ (Figure S4, left, Supporting Information). However, attempts to refine these cation positions failed – probably due to disorder – so that they were omitted in the final refinements. In further experiments discussed below, the existence of this cation was confirmed, which is known to be formed by hydrolysis of DMF under acidic conditions.[34,35] To account for the electron density of these cations as well as disordered solvent molecules in the pores of UoC-3, which could not be localized in difference Fourier maps, the SQUEEZE[28] option within PLATON[29] was used. It resulted in 692 electrons within the solvent accessible pores of UoC-3(DMF), **1** (for details see Table 2). After subtraction of four counter

cations (4 x 27 electrons), the remaining electrons are in reasonable agreement with four DMF molecules per formula unit so that the composition of **1** is described as $[(CH_3)_2NH_2][UO_2(3F\text{-}BTB)] \cdot 4$ DMF in the following. Using DEF as solvent, a MOF with the same topology is formed (cp. Figures S6 and S7, Table 2), denoted as UoC-3(DEF), **2**. Here, $[(C_2H_5)_2NH_2]^+$ cations (43 electrons) should be formed upon hydrolysis (cp. Figure S4, right, Supporting Information). SQUEEZE calculations result in 618 electrons per solvent accessible voids. With the same considerations, a composition $[(C_2H_5)_2NH_2][UO_2(3F\text{-}BTB)] \cdot 2$ DEF is deduced. This is in good agreement with the larger spatial requirements of $[(C_2H_5)_2NH_2]^+$ cations and DEF solvent molecules. However, at this point other solvents like water cannot be excluded to reside within the pores of **1** and **2**.

In the following, only the crystal structure of UoC-3(DMF), **1**, will be discussed in more detail. It is already obvious from Figure 1 that the uranyl unit forms a hexagonal bipyramid (the asymmetric unit of **2** is given in Figure S5, Supporting Information). The two symmetry equivalent oxygen atoms of the uranyl unit (U1-O1 = 1.755(8) Å) form the two apices of the bipyramid, whereas the base is formed by six oxygen atoms stemming from three carboxylate groups of three different *3F*-BTC^{3-} ligands. They form an almost ideal hexagon with U1-O distances ranging from 2.470(6) Å to 2.473(6) Å and O-U1-O angles in the range 53.0(2)° - 67.7(2)° (Table 3). The angular sum of 361.7° indicates an almost ideal planarity of the base of the hexagonal bipyramid. Very similar U-O distances and O-U-O angles are found for **2** with $[(C_2H_5)_2NH_2]^+$ as counter cation (Table 3).

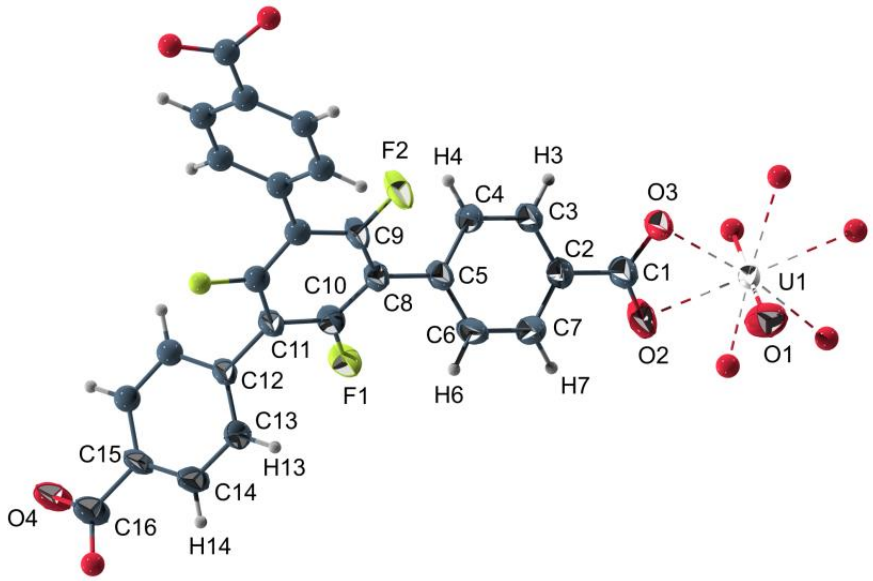

Figure 1. ORTEP plot of the crystal structure of UoC-3(DMF), **1**, with labelling of the atoms in the asymmetric unit. Thermal ellipsoids are drawn at the 50 % probability level. The *3F*-BTB^{3-} linker and the coordination sphere around U1 are completed by atoms drawn in a ball-and-stick presentation.

These $[UO_2]^{2+}$ units are connected by the *3F*-BTB^{3-} linkers to form a 3D-framework structure. This is remarkable, as in the uranyl coordination polymer with the pristine BTB^{3-} linker a coordination polymer with a layered structure was observed.[10] A detailed analysis of the torsion angles in $[(CH_3)_2NH_2][UO_2(BTB)]\cdot DMF\cdot 6.5H_2O$[10] shows that the angles between the inner ring and the benzoate rings range from 22.3° to 26.7°, so that the BTB^{3-} linker cannot be considered as being planar in this compound. However, the rotation between the carboxylate groups and the benzoate rings is always opposite to the rotation between the inner ring and the benzoate substituents so that in sum, small torsion angles between the carboxylate groups and the inner ring ranging from 4.3° to 16.4° result. This leads to the observed formation of polymeric layers with a slight corrugation. For **1** the situation is different (Figure 2). Here, significantly larger torsion angles between the inner ring and the benzoate rings (40.3° - 63.9°) are observed due to steric repulsion between the benzoate rings and the fluoro substituents. For two of them (symmetry-

equivalent), the rotation of the carboxylate group occurs in the opposite direction decreasing this torsion to an overall angle of ~12.9°. However, for the third benzoate group the phenyl ring and the carboxylate group rotate in the same direction, so that an almost perpendicular "out of plane" arrangement of the carboxylate group with respect to the inner ring is found (84.7°, Table 3). This structural behavior of the *3F*-BTC^{3-} linker is emphasized in Figure 2. It leads to the formation of a 3D-connected framework structure in contrast to $[(CH_3)_2NH_2][UO_2(BTB)]\cdot DMF\cdot 6.5H_2O$.[10] A similar behavior was observed for the *Me3*-BTB^{3-} linker in NU-1301.[12] We did not analyze the many organic linkers in this compound (816 linkers per unit cell), but refer to the published data that show an "out of plane" arrangement of these linkers.[12]

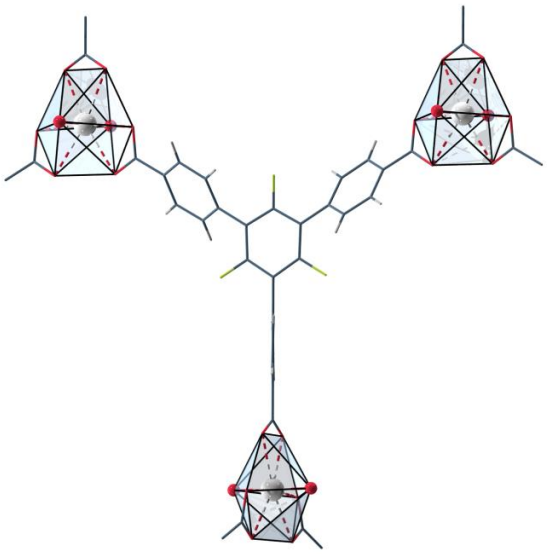

Figure 2. Coordination of the *3F*-BTB^{3-} linker in the crystal structure of UoC-3(DMF), **1**, emphasizing the tilting of the three benzoate rings with respect to the central *3F*-phenyl ring. The coordination sphere around U1 is shown as a light blue polyhedron. Color code: U (white), O (red), C (dark grey), F (green), H (light grey).

In **1**, the *3F*-BTB^{3-} linker connects the $[UO_2]^{2+}$ units to a 3D-framework structure with large porous channels along [010] (Figure 3) with an oval shape (size: approx. 10 x 8 Å). Along [100] (Figure S2, Supporting Information) and along [001] (Figure S3, Supporting Information) a more or less

dense packing is observed, so that UoC-3 (**1**) can be classified as a MOF with a 1D porous channel system. It should be noted that estimation of the sizes of these channels is difficult, as the counter cations $[(CH_3)_2NH_2]^+$ reside within these channels, which will minimize the accessible pore volumes. Probable positions of these cations were found in difference Fourier maps (Figure S4, Supporting Information) as already discussed above. To the best of our knowledge, UoC-3 (**1**) is one of the few examples of a MOF with uranyl nodes with a highly porous structure.[12,36]

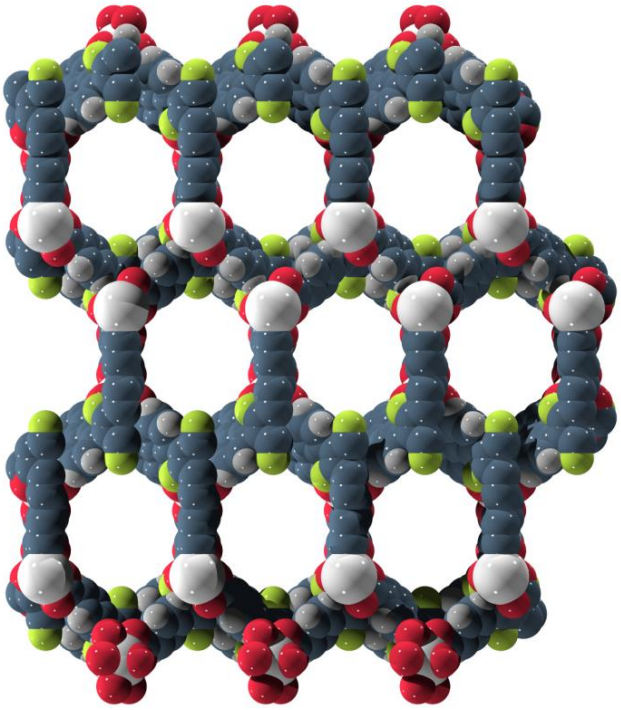

Figure 3. View of the crystal structure of UoC-3(DMF), **1**, in a projection along [010] showing large pores in this direction. Atoms are drawn with their respective van der Waals radii. Solvent molecules and $[Me_2NH_2]^+$ cations within the pores are omitted. Color code: U (white), O (red), C (dark grey), F (green), H (light grey).

A more detailed analysis of the UoC-3 anionic framework using ToposPro[37] reveals the *ths* ($ThSi_2$) topology, which is a relatively common uninodal 3-connected net (point symbol: 10^3). In UoC-3, four of these *ths* nets form a 4-fold interpenetrated structure, which is depicted in Figure 4. With

different counter cations (and solvent molecules inside the pores) no significant shifts of the lattice parameters were observed: a = 12.9279(5) Å, b = 11.5597(4) Å and c = 30.009(1) Å for **1** (measured at 290(2) K) compared to a = 12.9023(5) Å, b = 11.5845(4) Å and c = 30.001(1) Å for **2** (measured at 280(2) K, Table 2). This is in agreement with no significant shifts of the reflections in the PXRD patterns of these compounds (Figure S8, Supporting Information).

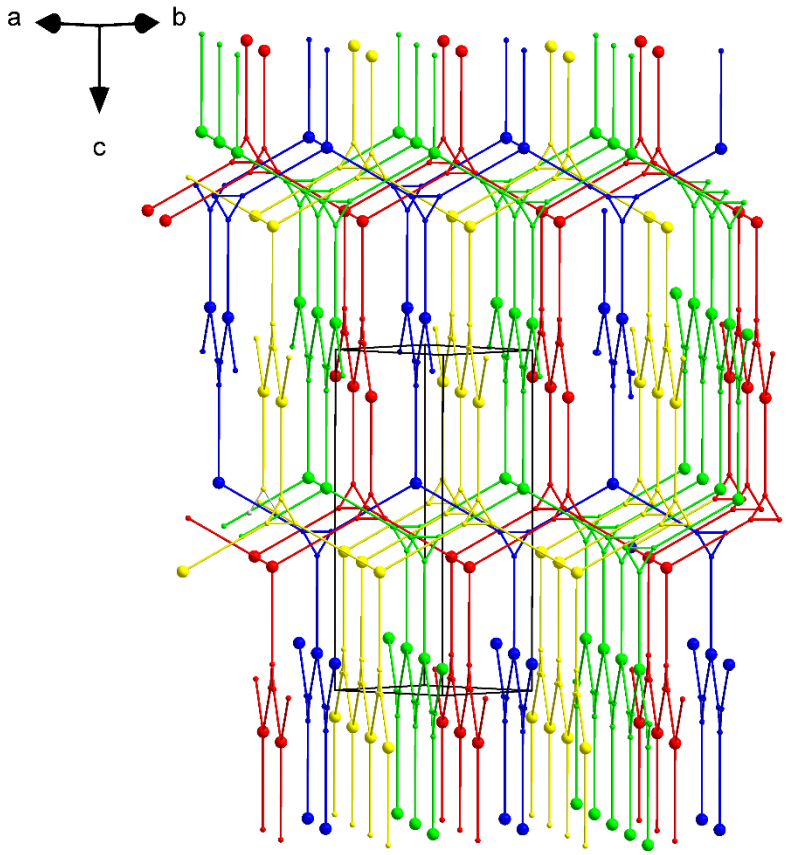

Figure 4. Four interpenetrating nets with *ths* ($ThSi_2$) topology in the crystal structure of **1**; each net is given in a different color.

To confirm the existence of $[Me_2NH_2]^+$ counter cations in the pores of **1**, which were assumed to be formed by hydrolysis of the DMF solvent,[34,35] it was attempted to synthesize **1** in an EtOH/H_2O solvent mixture and direct addition of $[Me_2NH_2]Cl$. The PXRD patterns clearly show that a MOF with the UoC-3 topology also forms under these synthetic conditions (cp. green and black patterns

in Figure 5). In a control experiment using an EtOH/H_2O solvent mixture without addition of $[Me_2NH_2]Cl$, only a yellow solution formed, from which a colorless solid precipitated, which was proven to be the unreacted linker.

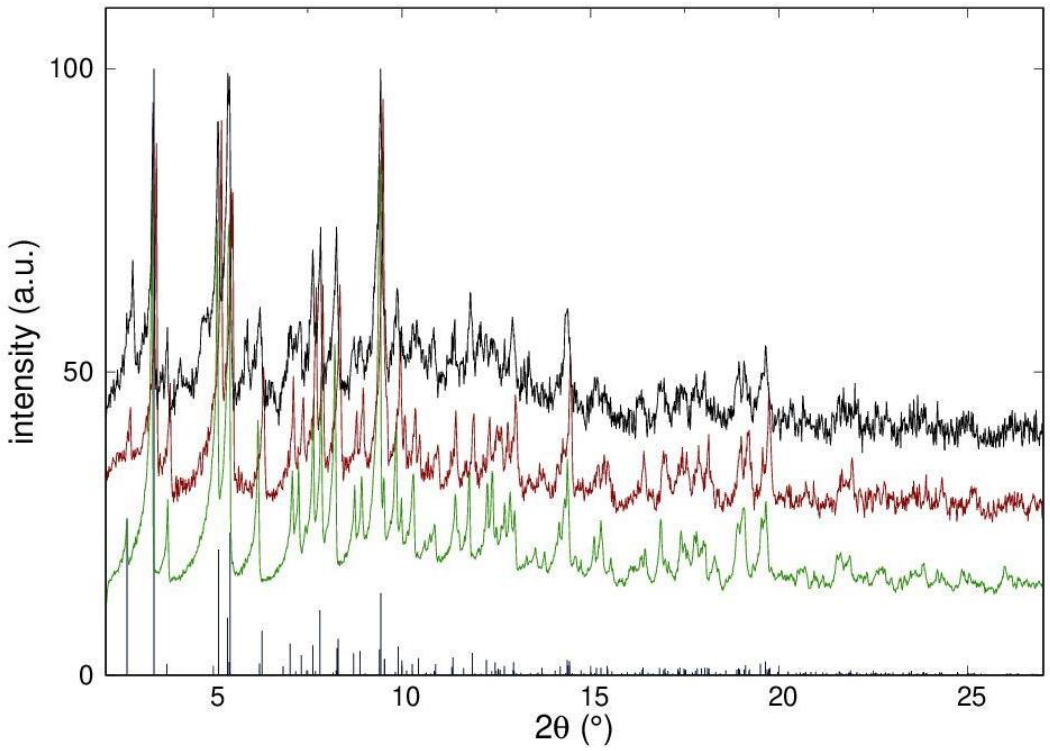

Figure 5. PXRD pattern of UoC-3(DMF) as-synthesized (**1**; green curve), UoC-3 after N_2 gas sorption measurement (red curve), and UoC-3 as obtained after reaction in EtOH/H_2O and addition of Me_2NH_2Cl (black curve). All data were collected on a Stoe Stadi P diffractometer (Mo Kα_1 radiation, Mythen detector). For comparison the theoretical pattern calculated from single crystal data of **1** is given as a blue line diagram.

IR/Raman spectroscopy is known to be a versatile tool to characterize $[UO_2]^{2+}$ units.[38,39] Whereas in the Raman spectra the symmetric O=U=O stretching vibration leads to a clearly visible signal at 810-880 cm^{-1} depending on the coordination sphere of the uranyl unit, in the IR spectra the asymmetric O=U=O stretching mode is observed in the range 915-960 cm^{-1} with carboxylate

ligands. In Figure 6 sections of the IR and Raman spectra of **1** are shown (700-1000 cm^{-1}; the complete IR and Raman spectra of **1** and **2** are given in Figure S16, Supporting Information). Both signals are found in the expected range: $\tilde{\nu}(O{=}U{=}O)_{sym}$ at 875 cm^{-1} in the Raman and $\tilde{\nu}(O{=}U{=}O)_{asym}$ at 917 cm^{-1} in the IR spectrum. It should be noted that the Raman spectrum is somewhat "noisy", but the respective signal is still clearly detectable. In former work on two coordination polymers with uranyl nodes and fluoro-substituted aromatic carboxylate ligands[17], we observed the symmetric O=U=O stretching vibration at slightly lower frequencies (851/852 cm^{-1}). More remarkable, in these compounds two completely different coordination spheres were observed, which lead to a splitting of the asymmetric O=U=O stretching vibration in the IR spectra with signals at 911/912 cm^{-1} and 929/928 cm^{-1}, whereas the symmetric O=U=O stretching mode (Raman) remained almost unaffected.[17] In the IR spectra of **1**, no splitting of the asymmetric O=U=O stretching vibration is detectable in agreement with only one, highly symmetric coordination sphere around the uranyl unit.

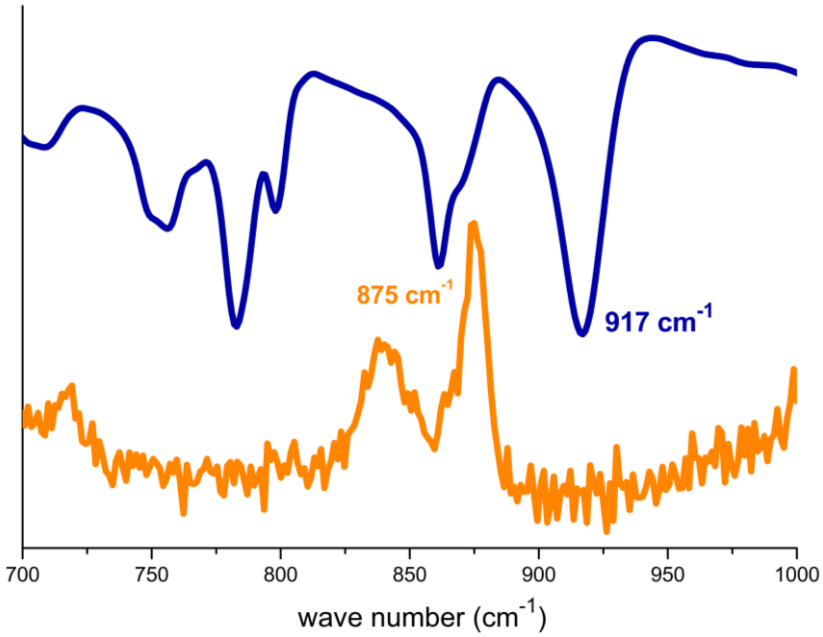

Figure 6. Section of the IR (blue) and Raman spectra (orange) of UoC-3(DMF), **1**. The wave numbers of the respective symmetric and asymmetric O=U=O stretching vibrations are indicated.

As already mentioned, MOFs with the UoC-3 topology are accessible in DMF or DEF as solvents, i.e. the formation of $[Me_2NH_2]^+$ or $[Et_2NH_2]^+$ cations has no significant structure-directing influence with the exception of some slight changes of the lattice parameters. Therefore, we investigated the influence of other solvents and their cations formed upon hydrolysis on the formation of MOFs with UoC-3 topology. With 1-formylpyrrolidine, which forms $[(C_4H_8)NH_2]^+$ cations with a heterocyclic structure, again a MOF with UoC-3 topology is obtained (Figure S9, Supporting Information). Even with DBF (*N*,*N*-di(*n*-butyl)formamide) forming large $[(n\text{-}C_4H_9)_2NH_2]^+$ cations, the formation of a MOF with the same topology is observed (Figure S10, Supporting Information). The PXRD patterns clearly confirm the formation of MOFs with the same topology, but they also show significant shifts of some reflections indicating lattice parameter changes upon embedment of cations with different shapes and sizes. Only after addition of the bulky $[(n\text{-}C_4H_9)_4N]^+$ cation (reaction of $UO_2(NO_3)_2 \cdot 6\ H_2O$ with H_3-*3F*-BTB and $[(n\text{-}C_4H_9)_4N]Br$ in an EtOH/H_2O solvent mixture), a completely different PXRD pattern was obtained. Unfortunately, we were unable to isolate single crystals suitable for an X-ray structure analysis from these reactions up to now. Currently, we are working on the optimization of the synthetic conditions to obtain samples with improved crystallinity.

The thermal stability and composition of UoC-3(DMF), **1**, was further explored by DSC/TGA. The results are depicted in Figure S17, Supporting Information. Assuming the composition $[(CH_3)_2NH_2][UO_2(3F\text{-BTB})] \cdot 4$ DMF, as concluded from the X-ray single-crystal structure analysis and subsequent SQUEZZE calculations, the release of four DMF molecules should lead to a mass loss of 26.6 %, which is reached at approx. 385 °C. However, there is no clear plateau

in the TGA curve and the DSC curve is almost featureless in this temperature range. As the TGA curve shows a small mass loss already at temperatures below 100 °C, the existence of water within the pores of UoC-3(DMF), **1**, is likely. Between 400-500 °C a second mass loss occurs (~4.7 %), before the decomposition of the material starts above 500 °C. This second mass loss might be due to the decomposition of the cation $[(CH_3)_2NH_2]^+$ under the release of dimethylamine, for which a mass loss of 4.1 % is calculated, although this decomposition temperature of the cation seems to be surprisingly high. Obviously, release of solvent molecules, decomposition of the cation and decomposition of the framework overlap with no clear plateau between them. Even at 1000 °C the decomposition seems to be not completed, although a PXRD pattern of the residue obtained after heating in the DSC/TGA clearly proofs the formation of UO_2 (Figure S14, Supporting Information).

For **2**, the composition $[(C_2H_5)_2NH_2][UO_2(3F\text{-BTB})] \cdot 2$ DEF was deduced from the X-ray single-crystal structure analysis and SQUEEZE calculations. Its DSC/TGA curves are given in Figure S18 (Supporting Information). Here, a mass loss of 19.5 % is calculated for the release of both DEF molecules, which is reached at approx. 285 °C. A small mass loss below 120 °C plausibly indicates the evaporation of water molecules present in the pores of **2**. Around 300 °C, another mass loss starts, which is accompanied by a small endothermic signal in the DSC curve. The decomposition of the $[(C_2H_5)_2NH_2]^+$ cation under the release of diethylamine should lead to a mass loss of 7.2 %, which is in reasonable agreement with the observed value. At approx. 500 °C, the decomposition of the framework starts accompanied by an endothermic signal.

For UoC-3(DBF), the composition is unknown. Its DSC/TGA curves are plotted in Figure S19 (Supporting Information). It displays the most pronounced signals in both DSC and TGA data. An almost flat TGA curve up to 120 °C obviously indicates that no water molecules reside in the pores

of this material. Above 130 °C, the release of DBF starts, accompanied by a very weak endothermic effect. In Figure 7, the TGA curves of **1**, **2**, and UoC-3(DBF) are plotted in one graphic. The release temperatures of DMF, DEF, and DBF nicely follow the trend of the boiling points of these solvents (b.p.(DMF) = 153 °C, b.p.(DEF) = 178 °C, b.p.(DBF) = 240 °C). For the release of one DBF molecule, a mass loss of 13.1 % is calculated. This value is reached around 300 °C. Above this temperature, two further events occur leading to another mass loss and two endothermic signals. For the release of dibutylamine by decomposition of the $[(C_4H_9)_2NH_2]^+$ cation, a mass loss of 10.7 % is expected. This obviously overlaps with the release of DBF. Therefore, the estimation of the composition of the material is difficult, but it should contain approx. 1.5 DBF molecules per formula unit, in good agreement with the rising spatial requirements of the solvent molecules (four DMF molecules in **1**, two DEF molecules in **2**, and 1.5 DBF molecules in UoC-3(DBF)). Between 400-450 °C, a plateau is reached in the TGA curve of UoC-3(DBF), before the decomposition of the framework starts at approx. 500 °C. Figure 7 shows that this decomposition is, as expected, very similar in all three remaining frameworks.

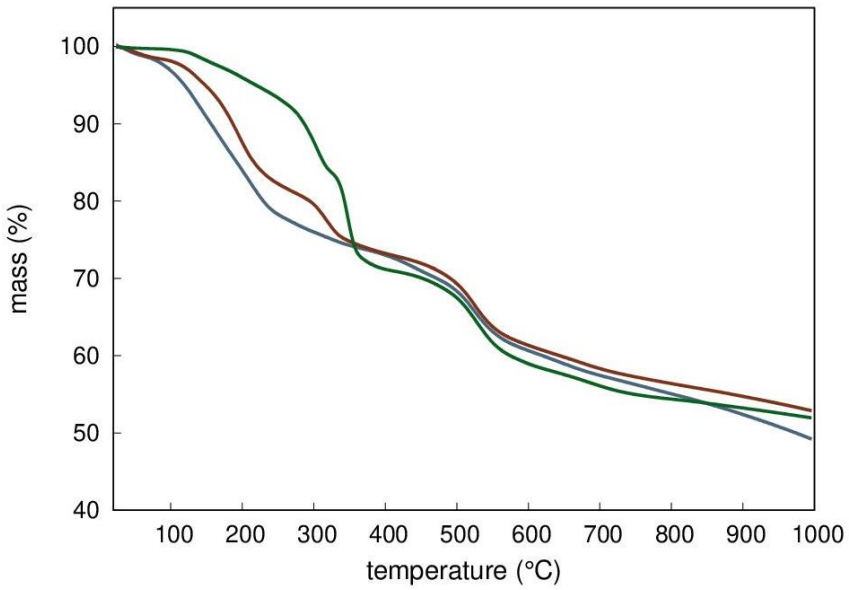

Figure 7. TGA curves of UoC-3(DMF) (**1**, blue line), UoC-3(DEF) (**2**, red line), and UoC-3(DBF) (green line).

The porosity of UoC-3(DMF), **1**, was confirmed by N_2 sorption measurements at 77 K. As expected from the TGA/DSC data (Figures 7 and S17), the search for the optimal activation conditions turned out to be difficult, as no clear plateau was visible in the TGA curve. In Figure S20 (Supporting Information), N_2 ad-/desorption isotherms recorded after different activation temperatures (always activated for 24 h) are depicted. The highest BET surface area was obtained after evacuation at 200 °C for 24 hours. As shown in Figure 5 (red curve), UoC-3 is still intact after activation with an unchanged crystallinity. The resulting ad-/desorption isotherm of **1** is depicted in Figure 8 (red curve). A type 1(a) isotherm characteristic for microporous materials was observed, resulting in a BET surface area of $S_{BET} = 4844$ m^2/g (for details see Experimental Section). For **2**, a smaller BET surface area of $S_{BET} = 3602$ m^2/g was measured (Figure 8, black curve; activation: Figure S21, Supporting Information), which can be explained by increased pore blockage of the larger $[(C_2H_5)_2NH_2]^+$ cations. Both S_{BET} values point to a highly porous MOF with BET surface areas comparable to those of other MOFs with uranyl nodes, namely NU-1300 ($S_{BET} = 2100$ m^2/g)[36] and NU-1301 ($S_{BET} = 4750$ m^2/g)[12], reported in the recent past.

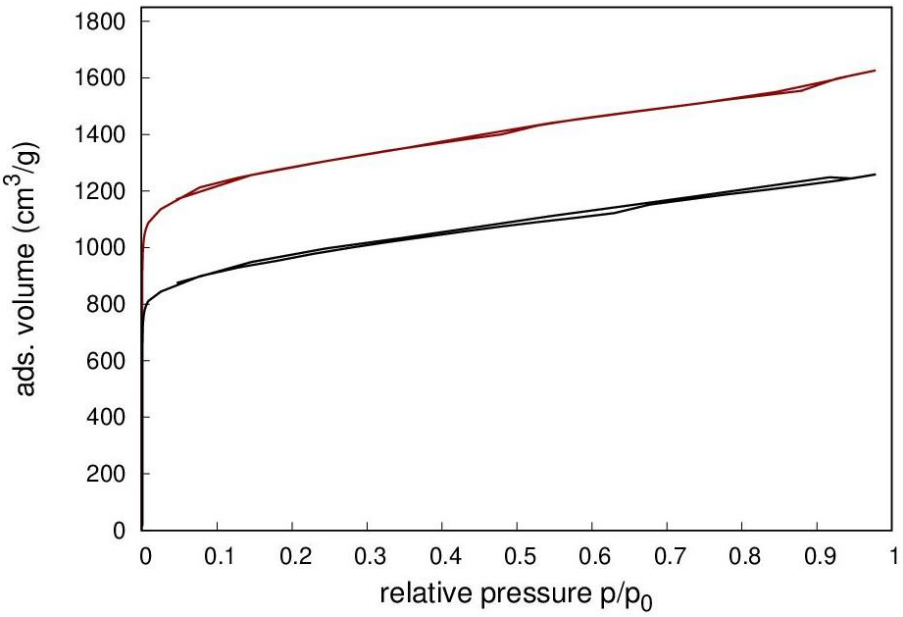

Figure 8. N_2 adsorption and desorption isotherms of UoC-3(DMF) (**1**, red curve) and UoC-3(DEF) (**2**, black curve), carried out at 77 K after activation at 200 °C for 24 h (**1**: S_{BET} = 4844 m^2/g; **2**: 3602 m^2/g).

As shown in Table 1, UoC-3 is also obtained from a solution containing $UO_2(NO_3)_2 \cdot 6\ H_2O$, H_3-*3F*-BTB, and KCl in an EtOH/H_2O solvent mixture. It clearly shows that K^+ is able to replace the organic cation $[R_2NH_2]^+$ in the synthesis. Therefore, we have also tested, whether K^+ can replace $[(CH_3)_2NH_2]^+$ in an ion exchange experiment. As UoC-3 turned out to be stable in water for longer times (Figure S15, Supporting Information), **1** and KCl were stirred in an aqueous solution for 48 h. After filtering off the precipitate and washing it with several portions of deionized water, it was analyzed by XPS (Figure 9).

Survey spectra of pristine UoC-3(DMF) (**1**) and the material obtained after exchange with KCl (Figure 9a)) show the expected peaks for the elements carbon, oxygen, fluorine, and uranium. Additionally, the K 2p peak is seen as a shoulder at higher binding energies of the C 1s peak in the KCl exchanged material. For a more detailed analysis, high-resolution spectra were recorded

(Figures 9b) and c)). In the range from 370 to 405 eV (Figure 9b)), the signals of the U 4f, N 1s, and K 2s orbitals strongly overlap. Nonetheless, by comparing the spectra of pristine UoC-3 and KCl exchanged UoC-3, the contribution of the K 2s peak (~372 eV) in the KCl exchanged material is clearly visible, whereas the N 1s peak (~399.4 eV) almost disappeared.[40,41] Moreover, the analysis of the U 4f signals confirm that uranium is, as expected, in valence state +VI due to a binding energy of 382.4 eV (U 4f 7/2), a spin-orbit splitting of ΔE = 11 eV, and its characteristic satellites features.[42,43] The final proof for the successful $[(CH_3)_2NH_2]^+$ vs. K^+ exchange can be given by analysis of the C 1s/K 2p region of the high-resolution XPS spectra (Figure 9c)). In general, carbon atoms with C=C and C-C bindings are fitted separately with a ΔE of ca. 0.3-0.8 eV. However, as obvious from Figure 9c) carbon-carbon bindings in UoC-3(DMF) (**1**) and the KCl exchanged material strongly overlap due to contributions from the *3F*-BTB^{3-} linker, DMF solvent molecules and the $[(CH_3)_2NH_2]^+$ cations, so that the C=C/C-C bindings were fitted as one peak and set to a binding energy of 284.8 eV. An additional peak associated to the π-π* satellite at ca. 290.8 eV is also visible and affirms the presence of sp^2 carbon atoms of the *3F*-BTB^{3-} linker.[44,45,46,47] While the peaks of the K 2p orbital are clearly visible in the KCl exchanged UoC-3 (K 2p 3/2: 294 eV; K 2p 1/2: 296.51 eV), the contributions of the C-H bindings (284.8 eV) decrease confirming a successful exchange of $[(CH_3)_2NH_2]^+$ by K^+.

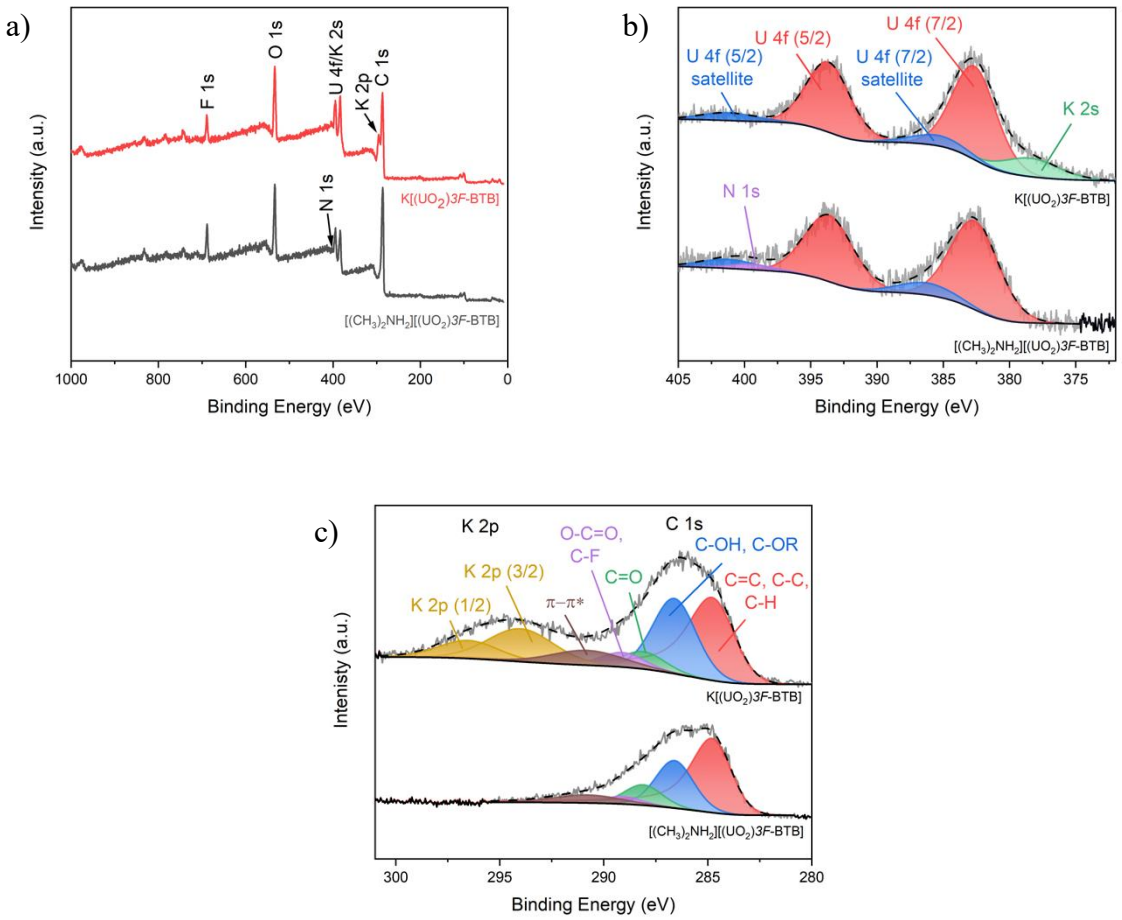

Figure 9. XPS analysis of pristine UoC-3(DMF) (**1**) and after exchange with KCl; a) survey spectra, b) high-resolution spectra with K 2s, U 4f, and N 1s peaks, c) high-resolution spectra with C 1s and K 2p peaks.

This successful cation exchange in UoC-3(DMF), **1**, motivated us to look for possible applications of the material. ^{137}Cs is a radioactive fission product of the nuclear fission of ^{235}U in nuclear reactors and weapons. Due to its high water solubility and its short-to-medium-lifetime $t_{1/2} = 30.17$ y, it is one of the most problematic radionuclides in nature. Its removal from aqueous solutions (i.e. sea water) is a real challenge and many materials were tested for this purpose.[48,49,50,51] The coordination polymer $[(CH_3)_2NH_2][UO_2(BTB)]\cdot DMF\cdot 6.5H_2O$ was also shown to selectively remove cesium from aqueous solutions[10] as well as the modified MOF MIL-

101-SO_3H.[52] As **1** showed a successful exchange of $[(CH_3)_2NH_2]^+$ cations by K^+, we also tested it for its Cs^+ exchange abilities. In a test experiment it was shown that the framework of UoC-3(DMF), **1**, is still intact after Cs^+ exchange with CsCl (Figure S13, Supporting Information).

Tests with a carrier-free solution of the radionuclide ^{137}Cs showed a successful exchange of Cs^+ cations with $[(CH_3)_2NH_2]^+$, demonstrating the principal usability of **1** for an effective removal of radiocesium from aqueous solutions. About 96% of the ^{137}Cs was adsorbed (K_d = 4390±280). After regeneration with a surplus of $[(CH_3)_2NH_2]^+$, the material exhibited an adsorption of 93% (K_d = 2620±240). We consider this a promising result, although this is not yet in the region of highly selective hexacyanoferrates that are used effectively e.g. to remove radionuclides from Fukushima Daiichi waste effluent.[53] An adsorption isotherm was determined by adding non-radioactive Cs as a carrier, indicating that the Cs^+ uptake is compatible with the assumption that the loaded form of **1** contains Cs/U in a ratio of ~1:4 (Figure S22, Supporting Information). In the presence of a surplus of Na^+/K^+ ions, high K_d values were obtained for Cs^+. We used Na^+/K^+ in a ratio as in seawater; the K_d values are starting to drop when $c(Na^+)/c(K^+)$ exceeds $1.8\cdot10^{-4}/5.0\cdot10^{-6}$ mol/L. Although this is below sea water concentrations, it still corresponds to a vast surplus of Na^+/K^+ ions, as the concentration of the used $^{137}Cs^+$ solution is only around 10^{-12} mol/L (see Table S1, Supporting Information).

CONCLUSIONS

By reaction of $UO_2(NO_3)_2 \cdot 6\ H_2O$ with H_3-*3F*-BTB in DMF/H_2O under solvothermal acidic conditions, the highly porous MOF UoC-3 ($[(CH_3)_2NH_2][UO_2(3F\text{-BTB})] \cdot 4$ DMF) with an anionic framework was obtained (S_{BET} = 4844 m^2/g), showing a 4-fold interpenetrated *ths* ($ThSi_2$)

topology. The charge compensating $[(CH_3)_2NH_2]^+$ cation is formed by hydrolysis of DMF. Reactions in DEF lead to the same MOF, but with charge compensating $[(C_2H_5)_2NH_2]^+$ cations (S_{BET} = 3602 m^2/g). Even with larger $[(n\text{-}C_4H_9)_2NH_2]^+$ cations the same topology was found. Only with the very large $[(n\text{-}C_4H_9)_4N]^+$ cation a completely different diffraction pattern was observed, indicating the formation of a solid with a new crystal structure. However, the crystallinity of this compound was too low to elucidate its crystal structure. UoC-3 is another example of uranium-based MOFs, which have attained a lot of attention in the recent past.[7,8,54,55,56,57,58]

UoC-3 is stable in water and its thermal decomposition under inert conditions occurs significantly above 400 °C. UoC-3 was successfully tested to remove ~96% radioactive $^{137}Cs^+$ from aqueous solutions by cation exchange, while retaining its crystal structure. The exchange also works in the presence of a larger surplus of Na^+ and K^+ cations, although not yet at seawater concentrations. At the moment, we are testing the Cs^+ exchange abilities of other coordination polymers with fluorinated aromatic carboxylate ligands, we have synthesized in the recent past. Furthermore, the easy exchangeability of cations in UoC-3 allows the targeted incorporation of functional cations, which is one of our primary research goals in this field in the near future.

From a structural point of view, it is remarkable that with the unfluorinated, almost planar BTB^{3-} linker a coordination polymer is formed with graphene-like layers.[10] Fluorination of the inner ring leads to a rotation of the benzoate groups out of the plane and thus the formation of a 3D-connected MOF. A similar finding was reported for a giant uranyl MOF (NU-1301), where the inner ring of the *Me3*-BTB^{3-} linker bears three methyl groups.[12] But it was also found that fluoro substituents may lead to a high degree of disorder of the benzoate groups in BTB^{3-} ligands.[59] According to the classification introduced by *Shustova* and co-workers[6] UoC-3 and NU-1301 belong to the MOFs with mononuclear motifs showing some similarities to minerals with $[UO_2(CO_3)_3]^{4-}$ cores.[60]

Currently, we are working on other examples of uranyl MOFs and coordination polymers with fluorinated aromatic polycarboxylate ligands. Especially the concept that fluoro substituents cancel the planarity of such linkers is intriguing and might pave the way for the synthesis of more uranyl MOFs with interesting structures and properties.

ASSOCIATED CONTENT

*Supporting Information

The Supporting Information is available free of charge on the ACS Publications website at DOI: 10.1021/acs...

Linker synthesis including NMR spectra (^{1}H, ^{13}C, ^{19}F), photograph of UoC-3 crystals, additional views of the crystal structure of UoC-3, experimental and simulated powder X-ray diffraction patterns, IR and Raman spectra, DSC/TGA diagrams, N_2 sorption and desorption isotherms after different conditions of activation, Cs^+ adsorption isotherm, data of γ spectrometry.

Accession Codes

CCDC 2053846 (**1** measured at 290(2) K), 2053847 (**2** measured at 103(2) K), and 2115257 (**2** measured at 280(2) K) contain the supplementary crystallographic data for this paper. These data can be obtained free of charge via www.ccdc.cam.ac.uk/data_request/cif, or by emailing data_request@ccdc.cam.ac.uk, or by contacting The Cambridge Crystallographic Data Centre, 12 Union Road, Cambridge CB2 1EZ, UK; fax: +44 1223 336033.

AUTHOR INFORMATION

Corresponding Author

Uwe Ruschewitz

*Tel.: (+49)221-470-3285.

Fax: (+49)221-470-3933.

E-mail: uwe.ruschewitz@uni-koeln.de.

ORCID

Uwe Ruschewitz: 0000-0002-6511-6894

Erik Strub: 0000-0002-4136-2871

Sanjay Mathur: 0000-0003-2765-2693

Notes

The authors declare no competing financial interest.

ACKNOWLEDGMENTS

We thank Dirk Pullem (elemental analysis, IR spectroscopy) and Dr. Christoph Lenting (Raman spectroscopy) for their help and the German Science Foundation (DFG) for financial support (Project No. RU 546/12-1).

Table 2. Details of X-ray single crystal structure analysis of **1** and **2**.

	$(Me_2NH_2)[(UO_2)(3F\text{-BTB})]\cdot xL$ (**1**) ≡ UoC-3(DMF)	$(Et_2NH_2)[(UO_2)(3F\text{-BTB})]\cdot xL$ (**2**) ≡ UoC-3(DEF)
Formula	$C_{27}H_{12}F_3O_8U$ [+ cation, + solvent]	$C_{27}H_{12}F_3O_8U$ [+ cation, + solvent]
Formula weight (g/mol)	759.40	759.40
Crystal description	Irregular, yellow	Irregular, yellow
Crystal size (mm)	0.15 · 0.20 · 0.20	0.15 · 0.10 · 0.10
Space group; Z	*Pnna* (no. 52); 4	*Pnna* (no. 52); 4
a (Å)	12.9279(5)	12.9023(5)
b (Å)	11.5597(4)	11.5845(4)
c (Å)	30.009(1)	30.001(1)
V (Å^3)	4484.7(3)	4484.1(3)
Absorption correction	Multi-scan (SADABS-2016/2)[24]	Multi-scan (SADABS-2016/2)[24]
Diffractometer, radiation	Bruker APEX-II CCD, Cu Kα	Bruker APEX-II CCD, Cu Kα
Temperature (K)	290(2)	280(2)
$2\theta_{max}$ (°)	144.39	144.90
Index ranges	$-15 \le h \le 15$; $-9 \le k \le 14$; $-36 \le l \le 30$	$-15 \le h \le 15$; $-14 \le k \le 14$; $-37 \le l \le 37$
Reflections collected / independent	30361 / 4422	63933 / 4440
Significant reflections	3709 with $I > 2\sigma(I)$	3933 with $I > 2\sigma(I)$
R(int)	0.0952	0.0746
Data / parameters / restraints	4422 / 180 / 0	4440 / 180 / 0
GooF = S_{all} (before SQUEEZE)	0.947 (1.210)	1.119 (1.198)
R [$I > 2\sigma(I^2)$] (before SQUEEZE)	0.0703 (0.0880)	0.0422 (0.0538)
wR(F^2), all data (before SQUEEZE)	0.1550 (0.1988)	0.1158 (0.1753)
Solvent accessible volume, electrons found in s.a.v. (SQUEEZE)	2427 Å^3, 692	2006 Å^3, 512
$\Delta\rho_{max}$ / $\Delta\rho_{min}$, e·10^{-6} pm^{-3}	-2.51 / 1.44	-1.115 / 1.214
CCDC deposition number	CCDC-2053846	CCDC-2115257

Table 3. Selected interatomic distances and angles in the crystal structures of **1** and **2**.

	$(Me_2NH_2)[(UO_2)(3F\text{-}BTB)]\cdot xL$ (**1**) ≡ UoC-3(DMF)	$(Et_2NH_2)[(UO_2)(3F\text{-}BTB)]\cdot xL$ (**2**) ≡ UoC-3(DEF)
U1-O1	1.755(8) Å, 2x	1.733(6) Å, 2x
U1-O3	2.470(6) Å, 2x	2.467(4) Å, 2x
U1-O4	2.472(5) Å, 2x	2.464(4) Å, 2x
U1-O2	2.473(6) Å, 2x	2.460(4) Å, 2x
O1-U1-O1	179.3(5)°	178.2(3)°
O1-U1-O2	84.9(4)°, 2x; 95.7(3)°, 2x	85.2(3)°, 2x; 96.3(3)°, 2x
O1-U1-O3	88.3(3)°, 2x; 91.8(3)°, 2x	89.5(2)°, 2x; 90.7(2)°, 2x
O1-U1-O4	87.2(3)°, 2x; 92.2(3)°, 2x	87.0(2)°, 2x; 91.3(2)°, 2x
O2-U1-O3	53.0(2)°, 2x	52.65(14)°, 2x
O4-U1-O4	53.2(3)°	52.6(2)°
O3-U1-O4	67.7(2)°, 2x	68.34(13)°, 2x
O2-U1-O2	67.1(3)°	67.0(2)°
Torsion angles of $3F\text{-}BTB^{3-}$ linker		
∠(inner ring – benzoate ring)	40.3°, 2x; 63.9°	39.3°, 2x; 63.7°
∠(benzoate ring – carboxylate group)	27.4°, 2x; 20.8°	27.4°, 2x; 20.2°
∠(inner ring – carboxylate group)	12.9°, 2x; 84.7°	12.2°, 2x; 83.9°

REFERENCES

(1) Li, H.; Eddaoudi, M.; O'Keeffe, M.; Yaghi, O. M. Design and Synthesis of an Exceptionally Stable and Highly Porous Metal-Organic Framework. *Nature* **1999**, *402*, 276–279.

(2) Chui, S. S. Y.; Lo, S. M. F.; Charmant, J. P. H.; Orpen, A. G.; Williams, I. D. A Chemically Functionalizable Nanoporous Material $[Cu_3(TMA)_2(H_2O)_3]_n$. *Science* **1999**, *283*, 1148–1150.

(3) Groom, C. R.; Bruno, I. J.; Lightfoot, M. P.; Ward, S. C. The Cambridge Structural Database. *Acta Crystallogr. Sect. B Struct. Sci. Cryst. Eng. Mater.* **2016**, *72*, 171–179.

(4) Moghadam, P. Z.; Li, A.; Wiggin, S. B.; Tao, A.; Maloney, A. G. P.; Wood, P. A.; Ward, S. C.; Fairen-Jimenez, D. Development of a Cambridge Structural Database Subset: A Collection of Metal–Organic Frameworks for Past, Present, and Future. *Chem. Mater.* **2017**, *29*, 2618–2625.

(5) Bruno, I. J.; Cole, J. C.; Edgington, P. R.; Kessler, M.; Macrae, C. F.; McCabe, P.; Pearson, J.; Taylor, R. New Software for Searching the Cambridge Structural Database and Visualizing Crystal Structures. *Acta Crystallogr. Sect. B Struct. Sci.* **2002**, *58*, 389–397.

(6) Dolgopolova, E. A.; Rice, A. M.; Shustova, N. B. Actinide-Based MOFs: A Middle Ground in Solution and Solid-State Structural Motifs. *Chem. Commun.* **2018**, *54*, 6472–6483.

(7) Lv, K.; Fichter, S.; Gu, M.; März, J.; Schmidt, M. An Updated Status and Trends in Actinide Metal-Organic Frameworks (An-MOFs): From Synthesis to Application. *Coord. Chem. Rev.* **2021**, *446*, 214011 (81 pages).

(8) Martin, C. R.; Leith, G. A.; Shustova, N. B. Beyond Structural Motifs: The Frontier of Actinide-Containing Metal–Organic Frameworks. *Chem. Sci.* **2021**, *12*, 7214–7230.

(9) Chae, H. K.; Siberio-Pérez, D. Y.; Kim, J.; Go, Y.; Eddaoudi, M.; Matzger, A. J.; O'Keeffe, M.; Yaghi, O. M. A Route to High Surface Area, Porosity and Inclusion of Large Molecules in Crystals. *Nature* **2004**, *427*, 523–527.

(10) Wang, Y.; Liu, Z.; Li, Y.; Bai, Z.; Liu, W.; Wang, Y.; Xu, X.; Xiao, C.; Sheng, D.; Diwu, J.; Su, J.; Chai, Z.; Albrecht-Schmitt, T. E.; Wang, S. Umbellate Distortions of the Uranyl Coordination Environment Result in a Stable and Porous Polycatenated Framework That Can Effectively Remove Cesium from Aqueous Solutions. *J. Am. Chem. Soc.* **2015**, *137*, 6144–6147.

(11) Go, Y. B.; Wang, X.; Jacobson, A. J. (6,3)-Honeycomb Structures of Uranium(VI) Benzenedicarboxylate Derivatives: The Use of Noncovalent Interactions to Prevent Interpenetration. *Inorg. Chem.* **2007**, *46*, 6594–6600.

(12) Li, P.; Vermeulen, N. A.; Malliakas, C. D.; Gómez-Gualdrón, D. A.; Howarth, A. J.; Mehdi, B. L.; Dohnalkova, A.; Browning, N. D.; O'Keeffe, M.; Farha, O. K. Bottom-up Construction of a Superstructure in a Porous Uranium-Organic Crystal. *Science* **2017**, *356*, 624–627.

(13) Seidel, C.; Lorbeer, C.; Cybińska, J.; Mudring, A.-V.; Ruschewitz, U. Lanthanide Coordination Polymers with Tetrafluoroterephthalate as a Bridging Ligand: Thermal and Optical Properties. *Inorg. Chem.* **2012**, *51*, 4679–4688.

(14) Sobieray, M.; Gode, J.; Seidel, C.; Poß, M.; Feldmann, C.; Ruschewitz, U. Bright Luminescence in Lanthanide Coordination Polymers with Tetrafluoroterephthalate as a Bridging Ligand. *Dalton Trans.* **2015**, *44*, 6249–6259.

(15) Krautwurst, J.; Smets, D.; Lamann, R.; Ruschewitz, U. How Does the Fluorination of the Linker Affect the Stability of Trimesate-Based Coordination Polymers and Metal–Organic Frameworks? *Inorg. Chem.* **2019**, *58*, 8622–8632.

(16) Stastny, C.; Ruschewitz, U. Two New MOFs Based on Cu_2 Paddlewheel Units and Biphenyltetracarboxylate Ligands with a Different Degree of Fluorination. *Z. Anorg. Allg. Chem.* **2018**, *644*, 1908–1914.

(17) Christoffels, R.; Ruschewitz, U. Two New Coordination Polymers with UO_2^{2+} Units and Fluorinated Aromatic Carboxylate Linkers. *Z. Anorg. Allg. Chem.* **2020**, *646*, 156–161.

(18) Smets, D.; Ruschewitz, U. How Does the Fluorination of the Linker Affect the Structural Chemistry of Trimesate-Based Metal-Organic Frameworks (MOFs)? *Z. Anorg. Allg. Chem.* **2020**, *646*, 1157–1167.

(19) Hulvey, Z.; Furman, J. D.; Turner, S. A.; Tang, M.; Cheetham, A. K. Dimensionality Trends in Metal−Organic Frameworks Containing Perfluorinated or Nonfluorinated Benzenedicarboxylates. *Cryst. Growth Des.* **2010**, *10*, 2041–2043.

(20) Wang, Z.; Kravtsov, V. C.; Walsh, R. B.; Zaworotko, M. J. Guest-Dependent Cavities in Two-Dimensional Metal−Organic Frameworks Sustained by Tetrafluoro-1,3-Benzenedicarboxylate. *Cryst. Growth Des.* **2007**, *7*, 1154–1162.

(21) Seidel, C.; Ahlers, R.; Ruschewitz, U. Coordination Polymers with Tetrafluoroterephthalate as Bridging Ligand. *Cryst. Growth Des.* **2011**, *11*, 5053–5063.

(22) Lamann, R.; Hülsen, M.; Dolg, M.; Ruschewitz, U. Syntheses, Crystal Structures and Thermal Behavior of Five New Complexes Containing 2, 4, 6-Trifluorobenzoate as Ligand. *Z. Anorg. Allg. Chem.* **2012**, *638*, 1424–1431.

(23) Yang, L.-M.; Fang, G.-Y.; Ma, J.; Pushpa, R.; Ganz, E. Halogenated MOF-5 Variants Show New Configuration, Tunable Band Gaps and Enhanced Optical Response in the Visible and near Infrared. *Phys. Chem. Chem. Phys.* **2016**, *18*, 32319–32330.

(24) Krause, L.; Herbst-Irmer, R.; Sheldrick, G. M.; Stalke, D. Comparison of Silver and Molybdenum Microfocus X-Ray Sources for Single-Crystal Structure Determination. *J. Appl. Crystallogr.* **2015**, *48*, 3–10.

(25) Altomare, A.; Cascarano, G.; Giacovazzo, C.; Guagliardi, A.; Burla, M. C.; Polidori, G.; Camalli, M. SIR 92 – a Program for Automatic Solution of Crystal Structures by Direct Methods. *J. Appl. Crystallogr.* **1994**, *27*, 435–435.

(26) Sheldrick, G. M. Crystal Structure Refinement with SHELXL. *Acta Crystallogr. Sect. C Struct. Chem.* **2015**, *71*, 3–8.

(27) Farrugia, L. J. WinGX and ORTEP for Windows : An Update. *J. Appl. Crystallogr.* **2012**, *45*, 849–854.

(28) Spek, A. L. PLATON SQUEEZE: A Tool for the Calculation of the Disordered Solvent Contribution to the Calculated Structure Factors. *Acta Crystallogr. Sect. C Struct. Chem.* **2015**, *71*, 9–18.

(29) Spek, A. L. Single-Crystal Structure Validation with the Program PLATON. *J. Appl. Crystallogr.* **2003**, *36*, 7–13.

(30) Brandenburg, K. *Diamond 3.2i*, Crystal Impact GbR, Bonn, Germany, 2012.

(31) *Win XPOW*, Version 3.12; Stoe & Cie GmbH: Darmstadt, Germany, 2018.

(32) *OriginPro*, Version 8.5.0G, OriginLab Corporation, Northhampton USA, 1991-2010.

(33) Alahakoon, S. B.; McCandless, G. T.; Karunathilake, A. A. K.; Thompson, C. M.; Smaldone, R. A. Enhanced Structural Organization in Covalent Organic Frameworks Through Fluorination. *Chem. - A Eur. J.* **2017**, *23*, 4255–4259.

(34) Cottineau, T.; Richard-Plouet, M.; Mevellec, J.-Y.; Brohan, L. Hydrolysis and Complexation of N , N - Dimethylformamide in New Nanostructurated Titanium Oxide Hybrid Organic–Inorganic Sols and Gel. *J. Phys. Chem. C* **2011**, *115*, 12269–12274.

(35) Burrows, A. D.; Cassar, K.; Friend, R. M. W.; Mahon, M. F.; Rigby, S. P.; Warren, J. E. Solvent Hydrolysis and Templating Effects in the Synthesis of Metal–Organic Frameworks. *CrystEngComm* **2005**, *7*, 548-550.

(36) Li, P.; Vermeulen, N. A.; Gong, X.; Malliakas, C. D.; Stoddart, J. F.; Hupp, J. T.; Farha, O. K. Design and Synthesis of a Water-Stable Anionic Uranium-Based Metal-Organic Framework (MOF) with Ultra Large Pores. *Angew. Chem., Int. Ed.* **2016**, *55*, 10358–10362.

(37) Blatov, V. A.; Shevchenko, A. P.; Proserpio, D. M. Applied Topological Analysis of Crystal Structures with the Program Package ToposPro. *Cryst. Growth Des.* **2014**, *14*, 3576–3586.

(38) Bullock, J. I. Raman and Infrared Spectroscopic Studies of the Uranyl Ion: The Symmetric Stretching Frequency, Force Constants, and Bond Lengths. *J. Chem. Soc. A* **1969**, 781-784.

(39) Kakihana, M.; Nagumo, T.; Okamoto, M.; Kakihana, H. Coordination Structures for Uranyl Carboxylate Complexes in Aqueous Solution Studied by IR and Carbon-13 NMR Spectra. *J. Phys. Chem.* **1987**, *91*, 6128–6136.

(40) Moulder, J. F.; Chastain, J. *Handbook of X-Ray Photoelectron Spectroscopy: A Reference Book of Standard Spectra for Identification and Interpretation of XPS Data*; Physical Electronics Division, Perkin-Elmer

Corporation, 1992.

(41) Xu, L.; Salmeron, M. An XPS and Scanning Polarization Force Microscopy Study of the Exchange and Mobility of Surface Ions on Mica. *Langmuir* **1998**, *14*, 5841–5844.

(42) Delobel, R.; Baussart, H.; Leroy, J.-M.; Grimblot, J.; Gengembre, L. X-Ray Photoelectron Spectroscopy Study of Uranium and Antimony Mixed Metal-Oxide Catalysts. *J. Chem. Soc., Faraday Trans. 1* **1983**, *79*, 879–891.

(43) Allen, G. C.; Holmes, N. R. Surface Characterisation of α-, β-, γ-, and δ-UO_3 Using X-Ray Photoelectron Spectroscopy. *Dalton Trans.* **1987**, 3009–3015.

(44) Phaner-Goutorbe, M.; Sartre, A.; Porte, L. Soft Oxidation of Graphite Studied by XPS and STM. *Microsc. Microanal. Microstruct.* **1994**, *5*, 283–290.

(45) Jackson, S. T.; Nuzzo, R. G. Determining Hybridization Differences for Amorphous Carbon from the XPS C 1s Envelope. *Appl. Surf. Sci.* **1995**, *90*, 195–203.

(46) Barinov, A.; Malcioğlu, O. B.; Fabris, S.; Sun, T.; Gregoratti, L.; Dalmiglio, M.; Kiskinova, M. Initial Stages of Oxidation on Graphitic Surfaces: Photoemission Study and Density Functional Theory Calculations. *J. Phys. Chem. C* **2009**, *113*, 9009–9013.

(47) Okpalugo, T. I. T.; Papakonstantinou, P.; Murphy, H.; McLaughlin, J.; Brown, N. M. D. High Resolution XPS Characterization of Chemical Functionalised MWCNTs and SWCNTs. *Carbon* **2005**, *43*, 153–161.

(48) Yi, R.; Ye, G.; Wu, F.; Wen, M.; Feng, X.; Chen, J. Highly Efficient Removal of ^{137}Cs in Seawater by Potassium Titanium Ferrocyanide Functionalized Magnetic Microspheres with Multilayer Core–Shell Structure. *RSC Adv.* **2014**, *4*, 37600–37608.

(49) Nenoff, T. M.; Krumhansl, J. L. Cs^+ Removal from Seawater by Commercially Available Molecular Sieves. *Solvent Extr. Ion Exch.* **2012**, *30*, 33–40.

(50) Kim, I.; Yang, H.-M.; Park, C. W.; Yoon, I.-H.; Seo, B.-K.; Kim, E.-K.; Ryu, B.-G. Removal of Radioactive Cesium from an Aqueous Solution via Bioaccumulation by Microalgae and Magnetic Separation. *Sci. Rep.* **2019**, *9*, 10149 (7 pages).

(51) Yang, H.-M.; Jang, S.-C.; Hong, S. B.; Lee, K.-W.; Roh, C.; Huh, Y. S.; Seo, B.-K. Prussian Blue-Functionalized Magnetic Nanoclusters for the Removal of Radioactive Cesium from Water. *J. Alloys Compd.* **2016**, *657*, 387–393.

(52) Aguila, B.; Banerjee, D.; Nie, Z.; Shin, Y.; Ma, S.; Thallapally, P. K. Selective Removal of Cesium and Strontium Using Porous Frameworks from High Level Nuclear Waste. *Chem. Commun.* **2016**, *52*, 5940–5942.

(53) Lehto, J.; Koivula, R.; Leinonen, H.; Tusa, E.; Harjula, R. Removal of Radionuclides from Fukushima Daiichi Waste Effluents. *Sep. Purif. Rev.* **2019**, *48*, 122–142.

(54) Liu, C.; Wang, C.; Sun, Z.-M. Conformational 2-Fold Interpenetrated Uranyl Supramolecular Isomers Based on (6,3) Sheet Topology: Structure, Luminescence, and Ion Exchange. *Inorg. Chem.* **2018**, *57*, 15370–15378.

(55) Liu, C.; Yang, X.-X.; Niu, S.; Yi, X.-Y.; Pan, Q.-J. Occurrence of Polyoxouranium Motifs in Uranyl Organic Networks Constructed by Using Silicon-Centered Carboxylate Linkers: Structures, Spectroscopy and Computation. *Dalton Trans.* **2020**, *49*, 4155–4163.

(56) Halter, D. P.; Klein, R. A.; Boreen, M. A.; Trump, B. A.; Brown, C. M.; Long, J. R. Self-Adjusting Binding Pockets Enhance H_2 and CH_4 Adsorption in a Uranium-Based Metal–Organic Framework. *Chem. Sci.* **2020**,

11, 6709–6716.

(57) Surbella, R. G.; Carter, K. P.; Lohrey, T. D.; Reilly, D.; Kalaj, M.; McNamara, B. K.; Schwantes, J.; Abergel, R. J. Rational Design of a Uranyl Metal–Organic Framework for the Capture and Colorimetric Detection of Organic Dyes. *Chem. – A Eur. J.* **2020**, *26*, 13819–13825.

(58) Jin, K.; Lee, B.; Park, J. Metal-Organic Frameworks as a Versatile Platform for Radionuclide Management. *Coord. Chem. Rev.* **2021**, *427*, 213473.

(59) Chen, T.-H.; Popov, I.; Kaveevivitchai, W.; Chuang, Y.-C.; Chen, Y.-S.; Jacobson, A. J.; Miljanić, O. Š. Mesoporous Fluorinated Metal-Organic Frameworks with Exceptional Adsorption of Fluorocarbons and CFCs. *Angew. Chem., Int. Ed.* **2015**, *54*, 13902–13906.

(60) Lussier, A. J.; Lopez, R. A. K.; Burns, P. C. A Revised and Expanded Structure Hierarchy of Natural and Synthetic Hexavalent Uranium Compounds. *Can. Mineral.* **2016**, *54*, 177–283.

TABLE OF CONTENTS Synopsis

By reaction of $UO_2(NO_3)_2 \cdot 6\ H_2O$ with H_3-*3F*-BTB in DMF/H_2O under solvothermal conditions the highly porous (S_{BET} = 4844 m^2/g) MOF UoC-3 ($[(CH_3)_2NH_2][UO_2(3F\text{-BTB})] \cdot 4$ DMF) with an anionic framework was obtained. The charge compensating $[(CH_3)_2NH_2]^+$ cation is formed by hydrolysis of DMF. Reactions in DEF lead to the same MOF, but with charge compensating $[(C_2H_5)_2NH_2]^+$ cations (S_{BET} = 3602 m^2/g). UoC-3 was successfully tested to remove ~96% radioactive $^{137}Cs^+$ from aqueous solutions by cation exchange, while retaining its crystal structure.

TABLE OF CONTENTS Graphic